



Original Article

# Li-Mn-Zn Supercapacitors for energy storage at high temperature of magnetic oxide thin films synthesized by SILAR method

D. D. Birajdar

Department of Physics, Shri Chhatrapati Shivaji College Omerga, Osmanabad (M.S.), India

**Manuscript ID:**  
RIGJAAR-2026-030209

ISSN: 2998-4459  
Volume 3  
Issue 2  
Pp. 46-50  
February 2026

**Submitted:** 08 Jan. 2026  
**Revised:** 15 Jan. 2026  
**Accepted:** 10 Feb. 2026  
**Published:** 28 Feb. 2026

**Correspondence Address:**  
D. D. Birajdar  
Department of Physics, Shri  
Chhatrapati Shivaji College  
Omerga, Osmanabad (M.S.),  
India  
Email:  
[damodar.birajdar@gmail.com](mailto:damodar.birajdar@gmail.com)

Quick Response Code:



Web: <https://rlgjaar.com>



DOI:  
10.5281/zenodo.20391239

DOI Link:  
<https://doi.org/10.5281/zenodo.20391239>



Creative Commons



## Abstract

Supercapacitors with their fast charge/discharge efficiency, good cycling life offer remarkable properties as energy storage devices compared to conventional energy storage systems. Li-Mn-Zn magnetic oxide thin films of composition  $Li_{1-x}Mn_{x/2}Zn_{0.5}Fe_{2-x/2}O_4$  ( $0.0 < x < 1$ ) are synthesized by SILAR method and sintered. Structural properties like X-ray diffraction, cation distribution and Infrared spectra studied. Dielectric properties such as dielectric constant, and dielectric loss factor are studied. It is observed that the thin films are spinel structured. The lattice constant increases with increase of Li contain. Due to enhancement of build-up of space charge polarization and because of that an increase in the dielectric properties.

**Keywords:** XRD, Supercapacitors, Thin films, SILAR

## Introduction

Supercapacitors are most suitable and innovative choice for green energy storage devices because of its fast recharge ability, high energy and power density, long cycle life and safe operation. Supercapacitors fulfill the gap between conventional capacitors and batteries. Global warming, environmental pollution, shortage of fossil fuel and increase in cost of it is economically not good. Because of less availability of nonconventional energy sources it is necessary to develop safe, green and clean energy sources [1]. In order to meet the demand of energy electronic battery is used in electronic vehicles and devices [2-4] but due to low power density and maintenance it is not convenient to use. Lithium-ion batteries, sodium-ion batteries, and supercapacitors has been attracted much attention, because they embrace the great potential in an extensive range of applications [8-10]. Different metal oxides like  $TiO_2$  [11],  $RuO_2$  [12],  $MnO_2$  [13],  $Fe_2O_3$  [14], are extensively studied as electrode materials for pseudo capacitors. Among these transition metal oxides,  $RuO_2$  is the most popular active material as supercapacitor electrodes because of its higher specific capacitance ( $2192 \text{ F g}^{-1}$  at  $2 \text{ mV s}^{-1}$  scan rate) with low ESR, good electrical conductivity, and broad potential window ( $0.0-1.0 \text{ V}$ ) [15,16]. The usage of thin film technology has transformed the area of electronics, optics, energy storage devices supercapacitors, sensors and magnetism, etc. [17-18]. The SILAR (Successive Ionic Layer Adsorption and Reaction) technique was reported for preparation of oxide thin films by Ristov et al. [19]. The capacitance depends on many conditions like method of synthesis, grain size and chemical composition. The ferrite materials are considered as potential electrodes in supercapacitor because of their low price, environmental benignity, different oxidation states, and their large abundance [20-24]. Their synthesis process is simple and suitable for production at industrial scale.  $MFe_2O_4$  ( $M = Mn, Co, Ni, Zn, \text{ or } Mg$ ) ferrites have been used in supercapacitor. These binary oxides can offer large capacitance due to involvement of two ions in redox reactions [25]. When the magnetic material is sintered under reducing condition the valence state changes and the individual cation is formed in the sample shows high conductivity when such material cooled in an oxygen atmosphere it is possible to form film of high resistivity [26].

## Experimental:

Thin films with general formula  $Li_{0.5}Mn_{x/2}Zn_{0.5}Fe_{2-x/2}O_4$  ( $0.0 < x < 1$ ) were prepared by SILAR method using the AR grade compounds  $Fe(NO_3)_3 \cdot 9H_2O$ ,  $Zn(NO_3)_2 \cdot 6H_2O$ ,  $Li(NO_3)_2 \cdot 4H_2O$ ,  $Cu(NO_3)_2 \cdot 6H_2O$ ,  $H_2C_2O_4 \cdot 2H_2O$  as starting materials.

## Creative Commons (CC BY-NC-SA 4.0)

This is an open access journal, and articles are distributed under the terms of the [Creative Commons Attribution-NonCommercial-ShareAlike 4.0 International Public License](https://creativecommons.org/licenses/by-nc-sa/4.0/), which allows others to remix, tweak, and build upon the work noncommercially, as long as appropriate credit is given and the new creations are licensed under the identical terms.

## How to cite this article:

Birajdar, D. D. (2026). Li-Mn-Zn Supercapacitors for energy storage at high temperature of magnetic oxide thin films synthesized by SILAR method. *Royal International Global Journal of Advance and Applied Research*, 3(2), 46-50. <https://doi.org/10.5281/zenodo.20391239>

Zinc nitrate, Manganese nitrate, Copper nitrate and Ferric nitrate were used as starting materials. Reaction procedure was carried out in air atmosphere without protection of inert gases. The molar ratio of metal nitrates to citric acid was taken as 1:3. The metal nitrates were dissolved in a minimum amount of double distilled water to get a clear solution and ammonia solution was slowly added to maintain the PH. The mixed solution was kept on to a hot plate with continuous stirring. The substrate was spin coated by the precursor solution at 3000rpm after that calcinated. This process was repeated for increasing the film thickness. Post-annealing of the precursor films was

performed in vacuum at 600°C for 4 hours to obtain  $\text{Li}_{0.5}\text{Mn}_x\text{Zn}_{0.5}\text{Fe}_{2-x/2}\text{O}_4$  films.

**Result and discussion:**

The X-ray diffraction patterns are obtained from Regaku miniflex II set up at the angle  $2^\circ/\text{m}$  in between  $20^\circ$  to  $80^\circ$ . Thin film samples were kept in the cavity for analysis at room temperature. The XRD patterns show peaks corresponding to Li-Mn-Zn ferrites and the absence of any other impurity phase. Substitution of Li by Mn increases the overall crystallinity of the spinel phase and all the peaks are indexed as reported on ASTM cards.

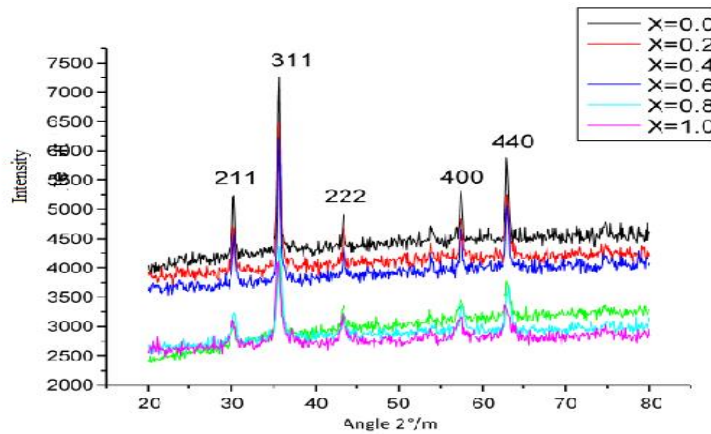


Figure 1. XRD patterns of  $\text{Li}_{0.5}\text{Mn}_x\text{Zn}_{0.5}\text{Fe}_{2-x/2}\text{O}_4$

The XRD patterns for present Mn doped thin films having thickness  $1\mu\text{m}$  were analyzed with comparing Li-Zn thin films. Compared samples shows simple cubic structure and also increase in 440 peak shows the increase in lattice constant. It show that the migration of  $\text{Li}^{2+}$  ions from octahedral to tetrahedral site. The cation distribution in the

present system was obtained from the analysis of X-ray diffraction patterns. In this method the observed intensity ratios were compared with the calculated intensity ratios. In the present study Bertaut method is used to determine the cation distribution [28]. This method selects a few pairs of reflections according to the expression.

$$\frac{I_{hkl}^{Obs.}}{I_{h'k'l'}^{Obs.}} \propto \frac{I_{hkl}^{Calc.}}{I_{h'k'l'}^{Calc.}} \tag{1}$$

X Composition	$d_{AX}$ A°	$d_{BX}$ A°	Tetra Edge (A°)	Octa Edge (A°)
0	1.907	2,054	3.112	2.821
0.2	1.904	2.050	3.104	2.823
0.4	1.905	2.052	3.123	2.822
0.6	1.908	2.053	3.124	2.828
0.8	1.102	2.055	3.126	2.912
1.0	1.112	2.058	3.128	2.985

Table 1: Tetrahedral and octahedral bonds and edges

Where,  $I_{hkl}^{Obs.}$  and  $I_{hkl}^{Calc.}$  are the observed and calculated intensities for reflection (hkl), respectively. The atomic scattering factor for various ions was taken from the literature [29]. It should be added that the calculated integrated intensities are valid at  $0^\circ\text{K}$ . Since the observed values are obtained at room temperature, a suitable correction is in principle necessary for the precise comparison. The variation of mean ionic radius of the A-site ( $r_A$ ) and of the B-site ( $r_B$ ) with x.

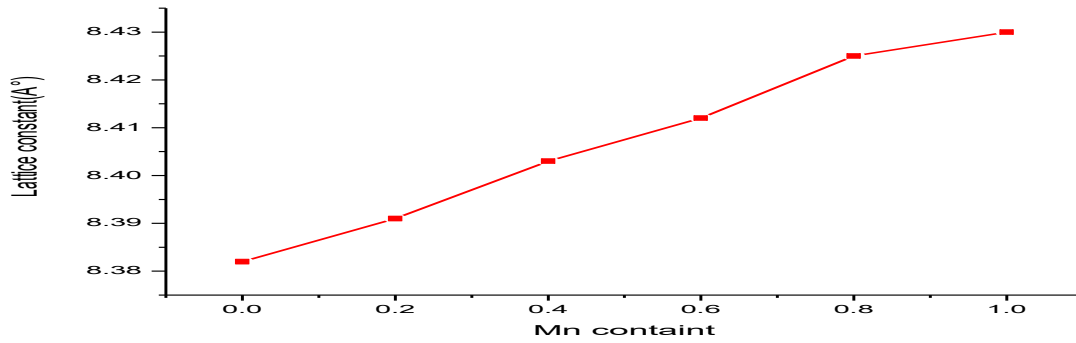


Figure 2. Lattice constant with increasing Mn<sup>3+</sup> ions.

Figure 3. IR spectra of  $\text{Li}_{0.5}\text{Mn}_{x/2}\text{Zn}_{0.5}\text{Fe}_{2-x/2}\text{O}_4$   $\text{cm}^{-1}$

Dielectric properties of prepared thin films depends on several factors like method of synthesis, Chemical composition etc. The sample mount used for measurement of capacitance and loss is shown in fig.

The capacitance bridge can be used for measurement of capacitance and dissipation factor. The dielectric constant of given sample is calculated by given formula i.e.

$$C = (C_o + C_s - C_m) / C_o$$

Where,

$C_s$ - measured capacitance

$C_o$ - geometrical capacitance

$C_m$ - capacitance of sample holder

$$\epsilon'' = \frac{\gamma - \gamma_{=}}{\epsilon' \omega} \quad (2)$$

Where,  $\gamma_{=}$  and  $\gamma$  are DC conductivity and AC conductivity respectively,  $\epsilon'$  is dielectric constant and  $\omega$  is frequency.

The approximation of experimental dependence was performed in accordance with equation.

$$\epsilon' = \epsilon'_{\infty} + \frac{\epsilon'_2}{h} \sum_{i=1}^n \frac{P_i D_i}{1 + \left(\frac{f}{f_{ki}}\right)^2} + \frac{\epsilon'_{st} \left[ 1 + \left(\frac{f}{f_t}\right)^m \cos \frac{m\pi}{2} \right]}{\left[ 1 + \left(\frac{f}{f_t}\right)^m \cos \frac{m\pi}{2} \right]^2 + \left[ \left(\frac{f}{f_t}\right)^m \sin \frac{m\pi}{2} \right]^2} \quad (3)$$

$$\epsilon' = \frac{\epsilon'_2}{h} \sum_{i=1}^n \frac{P_i D_i}{1 + \left(\frac{f}{f_{ki}}\right)^2} + \frac{\epsilon'_{st} \left(\frac{f}{f_t}\right)^m \sin \frac{m\pi}{2}}{\left[ 1 + \left(\frac{f}{f_t}\right)^m \cos \frac{m\pi}{2} \right]^2 + \left[ \left(\frac{f}{f_t}\right)^m \sin \frac{m\pi}{2} \right]^2} + \frac{\gamma_{=}}{\epsilon_0 \omega} \quad (4)$$

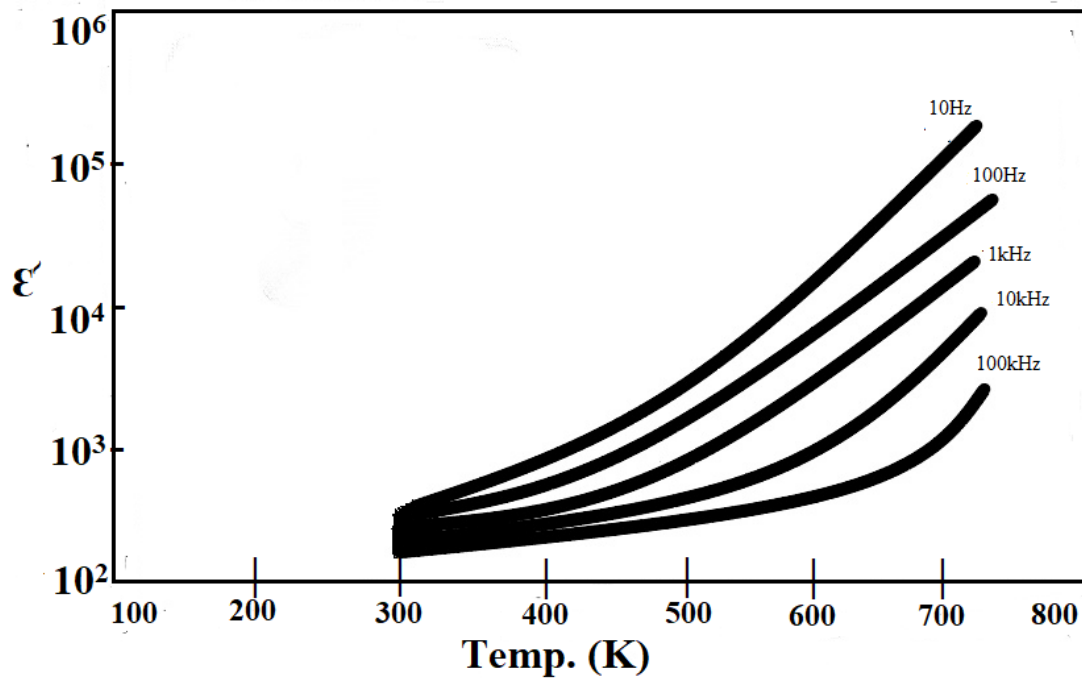


Figure 4. Increase in dielectric constant with temperature

The temperature dependence of dielectric constant is due to polarization effect. The space-charge polarization is governed by the number of space-charge carriers. With the rise in temperature the number of carriers increases, resulting in an enhancement of build-up of space charge polarization and because of that an increase in the dielectric properties.

#### Conclusions:

This work suggests that high quality Magnetic oxide thin films can be prepared by SILAR method. The surface of these materials play major role in supercapacitors. These materials works on redox process. The X-ray diffraction confirms the spinal structure of material. IR spectra confirms the spinel structure and gives information about the distribution of ions between tetrahedral site and octahedral site. With the rise in temperature the number of carriers increases, resulting in an enhancement of build-up of space charge polarization and because of that an increase in the dielectric properties.

#### Acknowledgment

The author expresses sincere gratitude to the Department of Physics, Shri Chhatrapati Shivaji College, Omerga, for providing the necessary research facilities and support to carry out this work.

Special thanks are extended to colleagues and laboratory staff for their valuable assistance during the experimental work and characterization studies.

#### Financial support and sponsorship

Nil.

#### Conflicts of interest

The authors declare that there are no conflicts of interest regarding the publication of this paper.

#### References:

1. J. H. Kim, K. H. Lee, L. J. Overzet, G. S. Lee, *Nano Lett.*, 11, (2011).
2. H. Ning, J. H. Pikul, R. Zhang, X. Li, S. Xu, J. Wang, J. A. Rogers, William P. King, and Paul V. Braun "Holographic patterning of highperformance on-chip D lithium-ion microbatteries" *Proceedings of the National Academy of Sciences*, vol. 112, no. 21, 6573-6578, 2015, doi: 10.1073/pnas.1423889112
3. N. Nitta, F. Wu, J. T. Lee, and G. Yushin, "Li-ion battery materials: Present and future," *Mater. Today*, vol. 18, no. 5, pp. 252-264, 2015, doi: 10.1016/j.mattod.2014.10.040.
4. H. J. Kim et al., "A comprehensive review of li-ion battery materials and their recycling techniques", vol. 9, no. 7, 1161, 2020, doi: org/10.3390/electronics9071161.
5. D. G. Gromadskyi, J. H. Chae, S. A. Norman, G. Z. Chen, *Appl. Energy*, 159, (2015), 39-50.
6. H. Jung, H. Wang, T. Hu, *J. Power Sources*, 267, (2014), 566-575.
7. S. Maiti, A. Pramanik, S. Chattopadhyay, G. De, S. Mahanty, *J. Colloid Interf. Sci.*, 464, (2016), 73-82.
8. H. Zhou, Y. Zhong, Z. He, L. Zhang, J. Wang, J. Zhang, C. Cao, *J. Alloys Compd.*, 597, 1-7(2014).
9. U. M. Patil, S. B. Kulkarni, V. S. Jamadade, C. D. Lokhande, *J. Alloys Compd.* 509, (2011).
10. V. J. Mane, D. B. Malavekar, S. B. Ubale, V. C. Lokhande, C. D. Lokhande, *Inorg. Chem. Commun.*, 115, (2020).
11. P. M. Kulal, D. P. Dubal, C. D. Lokhande, V. J. Fulari, *J. Alloys Compd.*, 509, (2011).
12. A. D. Jagadale, V. S. Kumbhar, R. N. Bulakhe, C. D. Lokhande, *Energy J.*, 64, (2014).



13. U. M. Patil R. R. Salunkhe, K. V. Gurav, C. D. Lokhande, Appl. Surf. Sci., 255, (2008).
14. S. Jeon, J. H. Jeong, H. Yoo, H. K. Yu, B. H. Kim, M. H. Kim, ACS Appl. Nano Mater., 3, (2020).
15. B. Y. Fugare, B. J. Lokhande, Mater. Sci. Semicond. Process., 71, (2017).
16. X. Cui, Y. Xu, X. Zhang, X. Cheng, S. Gao, H. Zhao, L. Huo, Sensor Actuat B-Chem, 247, (2017).
17. G. Brammertz, B. Vermang, H. ElAnzeery, S. Sahayaraj, S. Ranjbar, M. Meuris, J. Poortmans, Thin Solid Films, 616, (2016).
18. D. A. Minkov, G. M. Gavrilo, E. Marquez, S. M. Fernandez Ruano, A. V. Stoyanova, Optik, 132, (2017).
19. M. Ristov, Gj. Sinadinovski, I. Grozdanov, Thin Solid Films, 123, (1985).
20. X. Yao, J. Kong, D. Zhou, C. Zhao, R. Zhou, and X. Lu, "Mesoporous zinc ferrite / graphene composites: Towards ultra-fast and stable anode for lithium-ion batteries," Carbon, vol. 79, pp.493-499, 2014, doi: 10.1016/j.carbon.2014.08.007.
21. V. Venkatachalam and R. Jayavel, "Novel Synthesis of Ni-Ferrite (NiFe<sub>2</sub>O<sub>4</sub>) Electrode Material for Supercapacitor Applications," AIP Conference Proceedings, vol. 1665, no. 140016, 2015, doi: 10.1063/1.4918225.
22. P. V. Shinde, N. M. Shinde, R. S. Mane, and K. H. Kim, Chapter 5- Ferrites for Electrochemical Supercapacitors, Editor(s): Rajaram S. Mane, Vijaykumar V. Jadhav, In Micro and Nano Technologies, Spinel Ferrite Nanostructures for Energy Storage Devices, Elsevier, 2020, pages 83-122, ISBN 9780128192375, doi: org/10.1016/B978-0-12-819237-5.00005-5.
23. A. Soam, R. Kumar, D. Thatoi, and M. Singh, "Electrochemical Performance and Working Voltage Optimization of Nickel Ferrite/ Graphene Composite based Supercapacitor," J. Inorg. Organomet. Polym. Mater., vol. 30, no. 9, pp. 3325-3331, 2020, doi: 10.1007/s10904-020-01540-7.
24. S. Kuo and N. Wu, "Study on ferrites for supercapacitor application," 56<sup>th</sup> Annu. Meet. Int. Soc. Electrochem., no. December, (2015) 1-5.
25. S. F. Shaikh, M. Ubaidullah, R. S. Mane, and A. M. Al-Enizi, Chapter 4- Types, Synthesis methods and applications of ferrites, Editor(s): Rajaram S. Mane, Vijaykumar V. Jadhav, In Micro and Nano Technologies, Spinel Ferrite Nanostructures for Energy Storage Devices, Elsevier, 2020, Pages 51-82, ISBN 9780128192375, doi: org/10.1016/B978-0-12-819237-5.00004-3.
26. C.G. Koops, Phys. Rev., 83, 121., (1951).
27. L. Weil, E. F. Bertaut, L. Bochirol. J. Phys. Radium, 11, 208, (1950).
28. B.D. Cullity, Introduction to Magnetic Materials, Addison-Wesley, (1972)141.
29. Brabers V A M *Phys. Status Solidi* **33** 563, (1969).
30. Waldron R. D. *Phys. Rev.* **99** 1727, (1955).
31. Hafner S T Z. *Kristallogr.* **115** 331, (1961).